Synthesis of NiO/CuO nanocomposites using leaf extract from *Sapthodea campanulata* and its photocatalytic degradation of Methylene Blue under visible light Irradiation

Igneshgrace A[1], E.Sindhuja[1*]

[1]*PG and Research Department of Chemistry, Sri Paramakalyani College, Alwarkurichi, Affiliated to Manonmaniam Sundaranar University, Abishekapatti, Tirunelveli, Tamil Nadu, India.*

Corresponding author: sindhujaelangovan@gmail.com

Abstract:

Green synthesis of NiONPs, CuONPs and NiO/CuO nanocomposite were prepared by using hydrothermal method using *Sapthodea campanulata* leaf extract, which has been used as a stabilizing agent and reducing agent. *Sapthodea Campanulata* is widely available in India. The newly synthesized nanocomposites were characterized by various instrumental methods such as UV-vis spectroscopy (UV-vis), Fourier transform-infrared spectroscopy (FT-IR), and X-ray diffraction (XRD), scanning electron microscopy (SEM) and energy-dispersive X-ray spectroscopy (EDX), High Resolution-Transmission Electron microscope (HR-TEM). The nanocomposite shows a granular shape with face-centered cubic structure of CuO and NiO. The nanocomposites were photoactive and can be used efficiently as catalyst for degradation of Methylene blue (MB) under visible light irradiation at various times from 0 to 90 min. The percentage of degradation of efficiency was found to be 85%, 92%, 96% for NiO, CuO and NiO/CuO respectively. The higher MB degradation efficiency was exhibited by NiO/CuO nanocomposites (96%). The photocatalytic degradation of MB is based on a pseudo-first-order kinetic model and kinetic rate constant is higher for NiO/CuO nanocomposite (0.0884 min-1) than CuONPs (0.054 min^{-1}) and NiONPs (0.0234 min^{-1}). NiO/CuO nanocomposite proved a good photocatalyst and better stability for eliminating pollution in water. Using an agar well diffusion technique, CuO/NiO nanocomposite was recorded better anti-bacterial activities against both Zone of *(E.coli* for 20 mm) and (*S.aureus* for 18 mm) bacteria than ZnONPs and CuONPs.

Keywords: Green synthesis; *Sapthodea campanulata*; NiO/CuO nanocomposite; photocatalysis; visible light; Methylene blue dye;

1. Introduction

Methylene blue dye widely utilized in various industrial applications such as paper, textiles, leather, food, cosmetics and plastics. These factories discharge sewage into drinking water, polluting the water and creating high levels of toxins that could affect humans and animals [1]. MB has been a factor for many diseases like due to their toxicity, mutagenic ability, carcinogenicity, methemoglobinemia, confusion, vomiting and profuse sweating [2]. To overcome these problems, several methods have been developed for the removal of MB dye from water. These methods included adsorption, biosorption [3-6], coagulation [7], electrocoagulation [8], liquid-liquid extraction [9], ultrafiltration [10], biodegradation [11], plasma discharge [12], phytoremediation [13] and catalytic reactions [14].

The methods of treatments have suffered some disadvantages such as high cost, time-consuming, and less feasibility [15]. Nowadays, photocatalytic techniques are used for the degradation of MB dye at a low cost. The catalyst can be simply collected after the reaction. The advantages of these techniques are simple operation, complete degradation and mineralization [16]. Advance oxidation process (AOP) of photocatalyst method has been suggested for efficient treatment of waste water treatment using sun light under photocatalyst and this process can break down toxic molecule into non-toxic molecules under light irradiation [17]. Many types of semiconductor nanomaterials are used as photocatalysts such as TiO_2 [18], ZnO [19], ZnS [20], NiO [21], CuO [22], Fe_2O_3 [23], MnO [24], WO_3 [25], VO_4 [26] SnO_2 [27], CeO_2 [28], Co_3O_4 [29] n-type and p-type semiconductors has exhibited better degradation of dyes and organic pollutants from wastewater [30,31], However, these were shown to have a very high electron-holes recombination rate and have limited application.

Using metal oxide nanocomposites, the photocatalytic activity of metal oxides can be improved by reducing the electron-holes charge recombination rate and improving the activity under visible light irradiation. For these reason, various mixed metal oxides nanocomposites such as TiO_2/NiO, WO_3/ZnO, CuO/ZnO, Co_3O_4/NiO, ZnO/CeO_2 have been used to degrade organic pollutants under light exposure [32-35]. The above nanocomposites consisted of p-p, n-n and p-p heterojunction photocatalysts, in which the n-n and p-n heterojunction photocatalysts presented lower electron-holes recombination rate and more excellent photocatalytic activity under visible light irradiation [36]. CuO has p-type semiconductors show low bandgap energy,

low toxicity, cheap and its is widely used for the degradation of organic pollutants and other applications [37].

In the present work, CuO nanoparticles are coated with NiO (p-type semiconductors) with high bandgap energy to prepare CuO/NiO nanocomposite to improve the photocatalytic efficiency for degradation of organic pollutants [38, 39]. Recently, p-p type heterojunction such as CuO/ZnO, ZnO/NiO and NiO/CuO nanocomposites are being developed for the photocatlaytic degradation of organic dye under visible light irradiation, in which NiO/CuO nanocomposite showed better photocatalytic activity than both CuO/ZnO nanocomposite and ZnO/NiO nanocomposite [40]. Therefore, to our knowledge, CuO/NiO nanocomposite have not been reported for the photocatalytic degradation of organic dye.

In this research work, CuONPs, NiONPs, and NiO/CuO nanocomposite were prepared by using *Spathodea campanulata* extract by hydrothermal method. Which act as good stabilizing and reducing agent. The prepared metal oxides and metal oxides nanocomposite were characterized and used for photocatalytic degradation of MB blue dye under visible light irradiation. NiO/CuO nanocomposite showed a good photocatalytic degradation MB under visible light irradiation. Additionally, the materials were also tested for anti-bacterial activity against Escherichia coli (Gram-negative) and Staphylococcus aureus (Gram-positive) bacteria. The experimental findings showed that NiO/CuO had better antibacterial activity than ZnONPs and CuONPs against both (*S. aureus)* and (*E. coli*) bacteria.

2.0 Experimental Section

2.1 Chemicals reagents

Spathodea campanulata (leaves) were obtained near Sri Paramakalyani college, Alwarkurichi, in Tamil Nadu, India. Analytical grade copper sulfate pentahydrate ($CuSO_4.5H_2O$, 99 %), Nickel sulfate hexahydrate ($NiSO_4.6H_2O$, 99%), Methylene blue ($C_{16}H_{18}ClN_3S$) and ethanol were purchased from Sigma Aldrich Bangalore in India. Throughout the experiment, deionized water (DW) was used for washing and solution preparation.

2.2 Preparation of Plant Extract

The leaves of African tulip tree commonly known as *Spathodea campanulata*, were cleaned with distilled water and dried for two days to remove moisture.. Then the leaves were

dried, powdered and protected with an air bag. Heat 2.0 g of African tulip tree powder in 250 mL of distilled water with constant stirring at 80°Cfor 1hr. The solution was concentrated using rotavapour and then kept at 4°C [41].

2.3 Synthesis of CuONPs and NiONPs by using hydrothermal method

Preparation of CuONPs: 4.0 g (0.05M) of $Cu(NO_3)_2.3H_2O$ was stirred in 80 mL distilled water for 30 minutes and then added to 10 mL of extract and the solution was stirred for another 30 min. Then mixture of the solution was transferred into 100 mL, Teflon coated autoclave and heated in muffle furnace at 180°C for 6 hrs. After cooling the solution was centrifuged at 6000 rpm for 10 min to obtain a black precipitate, and then washed several times with water and ethanol to remove impurities. The precipitate was then dried at 100 °C to obtain a black powder. NiONPs were also synthesized under the above condition.

2.4 Synthesis of NiO/CuO nanocomposite by hydrothermal method

0.1M (2.0 g) of Cu $(NO_3)_2 \cdot 3H_2O$, 0.1M (2.0 g) of Ni $(NO_3)_2$. $6H_2O$ were added 80 mL distilled water and addition of 20 mL of extract solution was added and the solution is stirred for another 30 minutes at room temperature to obtain a homogenous mixture solution. The mixture was then poured into 100 mL Teflon coated autoclave and heated at 180 °C for 6hrs. After cooling the solution to room temperature, solution was centrifuged at 6000 rpm to obtain CuO/NiO nanocomposite [42, 43].

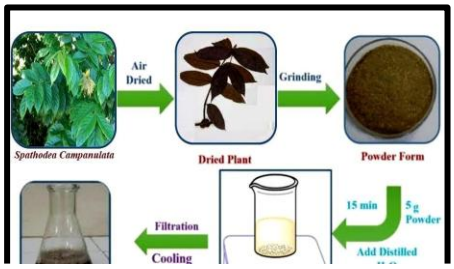

Scheme 1. Schematic diagram of the synthesis of extract from *Spathodea campanulata*

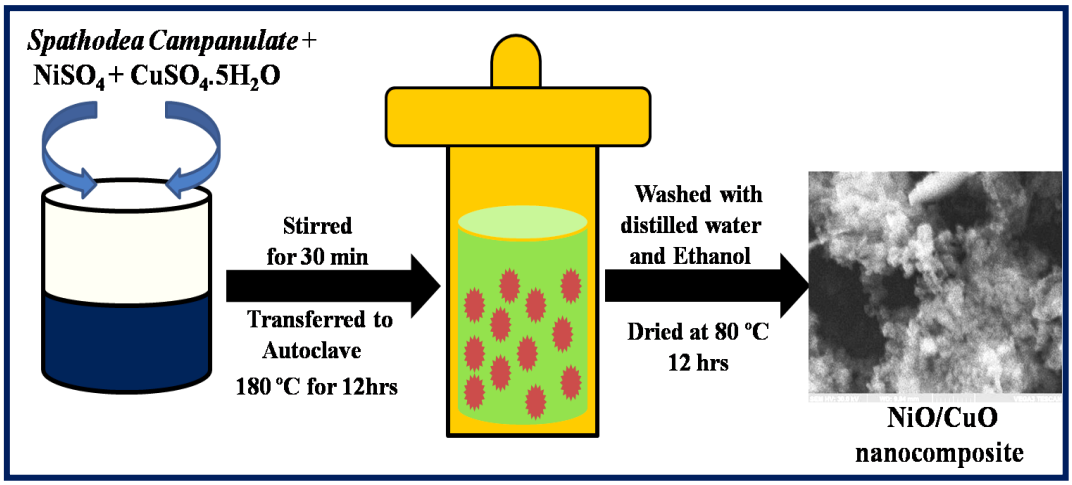

Scheme 2. Schematic diagram of the preparation of NiO/CuO nanocomposite by hydrothermal method

2.5 Characterization

The prepared nanomaterials of CuONPs, NiONPs and CuO/NiO nanocomposite were characterized using different instrument methods. UV-visible spectroscopy was used to characterize metal oxides and nanocomposite formation using UV-visible spectrophotometer (Hitachi UH-5300 spectrophotometer Double beam). Fourier transform infra red spectroscopy was performed using (Nicolet IS5R FTIR, KBR windows with AR Diamond crystal plate, Make: Thermofisher) for identify the function group in extract and metal oxides bond interaction. Crystalinity and phase purity of X-ray diffractometers (Bruker Eco D8 Advance) were investigated. The surface morphology and shape of metal oxide and metal oxides nanocomposite was studied by SEM (vega 3 Tescan). The elemental composition of metal oxides and metal oxide nanocomposite was determined by Energy-Dispersive X-ray (vega 3 Tescan). Using HR-TEM (Jeol, JEM 2100), the NPs' morphology was evaluated.

2.6 Photocatalytic degradation method

Photocatalytic degradation of MB with NiONPs, CuONPs, and NiO/CuO nanocomposite was conducted under visible light irradiation with the source of (250 W Xenon lamp, intensity 400 mW cm^{-2}), 10 ppm of MB in 100 mL water and 100 mg of NiONPs, CuONPs, and NiO/CuO nanocomposite was used as photocatalysts into the 1L glass tube. The center of the quartz glass tube was connected to a light lamp. The solution was kept under dark conditions for 30 min before visible light was illuminated to reach absorption-desorption equilibrium on the photocatalyst. This experiment was carried out at room temperature with visible light illumination. 10 mL of the degradation solution was collected at various time intervals with 0.45µM syringe filter to remove the photocatalysts. The concentration of the MB degradation solution was evaluated by using a UV-visible spectrophotometer (Shimadzu, UV-2450). The absorption peak of MB was determined at 674 nm [44].

Anti-bacterial assessment

The tools for the experiment were placed in an autoclave for 20 minutes at 121 °C. Before usage, Escherichia coli (E.coli) and Staphylococcus aureus (S.aureus) cultures were cultured in 50 ml of nutrient broth (NB) and incubated at 37 °C overnight before being used. The disc diffusion method was used to test the antibacterial activity of synthesised NiONPS, CuONPs, and NiO/CuO nanocomposite. After adding 20 ml of sterile Mueller Hinton Agar, 120 ml of bacterial culture was poured onto sterile petri plates and dispersed around with a spreader. On a 6 mm sterile disc, NiONPs, CuONPs, and a NiO/CuO nanocomposite were deposited. The loaded disc was placed on the medium's surface, and the extract was allowed to diffuse for five minutes before the plates were incubated for 24 hours at 37 °C. As a control, E.coli and Staphylococcus aureus (S.aureus) bacteria were mixed in with the solvents. [45, 46]. The inhibitory zones that had formed around the disc were measured in millimeters using a transparent ruler at the end of the incubation period.

3. Result and Discussion

3.1 UV-visible characterization

Figure 1A (a-d) shows the UV-visible spectra of (a) Extract, (b) CuONPs, (c) NiONPs, and CuO/NiO nanocomposite. Figure 1A (a) shows the extract exhibited two peaks, one with low intensity at 235 nm and 282 nm and another peak with strong intensity peak at 240 nm [47]. CuONPs showed higher intensity peak at 297 nm, corresponding to the phenolic groups of the

extract, and a broad peak at 406 nm due to the surface plasmon absorption of copper oxide nanoparticles [48]. This result was consistent with the report CuONPs as shown in Fig.1A (b) [49]. Figure (c) shows the NiONPs demonstrated two low intensity peaks at 335nm and 453 nm. Figure 1A(c) shows the broad peak at 341 nm due to reduced crystalline defect NiO with extract and an increase in temperature to improve the crystallinity and decrease the band gap energy [50,51]. Figure (d) showed the CuO-NiO nanocomposites absorption spectra. The formation of CuO-NiO nanocomposite was attributed to all metal oxide nanoparticle ratios that displayed weak peaks at 220 to 350 nm [52]. The absorption bands in the UV-Vis spectra confirmed the presence of CuO-NiO mixed oxides. Figure 1B (a-c) shows the Tauc plot of NiONPs, CuONPs, and NiO/CuO nanocomposite, where the NiO-CuO nanocomposite (2.76 eV) has a less band gap energy than the NiONPs (2.47 eV) and CuONPs (3.0 eV). The low band gap energy of the NiO/CuO nanocomposite resulted in excellent photocatalytic degradation activity under visible light irradiation [53].

3.2 FT-IR characterization

The FT-IR is used to determine the functional groups of compounds and the interaction at the surface of metal oxide and stabilizing agents. Figure 1B (a-d) shows the FT-IR spectra of (a) Extract, (b) CuONPs, (c) NiONPs, and (d) CuO/NiO nanocomposite. Figure 1B(a) shows the IR spectra taken. The spectra shows peaks at 3305 cm^{-1} (O-H bond stretching vibration), 2925 cm^{-1} and 2846 cm^{-1} (C-H bond stretching vibration CH_2 and CH groups), 1730 cm^{-1} (C=O stretching vibration in COOH groups and 1609 cm^{-1} (C=C stretching vibration) , at 1373 cm^{-1} (C=C bond stretching vibration), peak at 1016 cm^{-1} (C–O bond stretching vibration) [54]. CuONPs showed mostly low intensity peaks with slightly shifted peak position due to better interaction between extract and CuO, in which Cu-O bond stretching vibration at 571 cm^{-1} due to formation of CuONPs as shown in Fig.1B (b). [55]. Figure 1B(c) shows a small peak at 509 cm^{-1} corresponding to the stretching vibration of the Ni-O bond in the formation of NiONPs [56]. No unusual shift was observed in the peaks for CuO/NiO nanocomposite CuONPs and NiONPs, in which the CuONPs peak was slightly shifted to a higher wave number at 621 cm^{-1} due to effective coating on NiO as shown in Fig.1B (d).

3.3 XRD pattern characterization

The extract powder was showed three diffraction peaks at 2θ of 20.89° (100), 29.58° (002), and 41.20° (101) as shown in Fig.1C (a). Figure 1C (b) shows that the X-ray diffraction peaks of CuONPs at 2θ of 31.41° (110), 35.86° (11-1), 38.14° (111) and 45.37° (202). It was

evident to have monoclinic structure, which matches with JCPDS no. 00-048-1548 [57]. The XRD pattern of CuONPs shows that no additional peaks due to excellent crystallinity with excellent purity. Figure 1C(c) shows the NiONPs demonstrated multiple diffraction peak at 2θ of 38.14°, 43.94°, 62.08°, 75.84 and 78.15 ° corresponding to the (111), (200), (220), (311), and (222) crystallographic planes and planes of the face-centered cubic (FCC) according to JCPDS (JCPDS cared no. 00-047-1049) [58]. Figure 1C(d) shows that the appearance of better diffraction peaks due to the formation of CuO/NiO nanocomposite and CuO effectively coated on NiONPs [59]. These XRD results were used to determine the average crystallite size of nanomaterials by using Debye–Scherrer equation,

$$D=K\lambda/\beta \cos\theta \quad \text{..... (1)}$$

where K = 0.9, λ = 1.54056 Å(wavelength of Cu kα), D is the average crystallite size, β is the full-width half maximum (FWHM), and θ is the angle of diffraction. The crystalline size is obtained from high-intensity peaks of CuONPs (10.54 nm), NiO (22.25 nm), and CuO/NiO (28.42 nm), respectively.

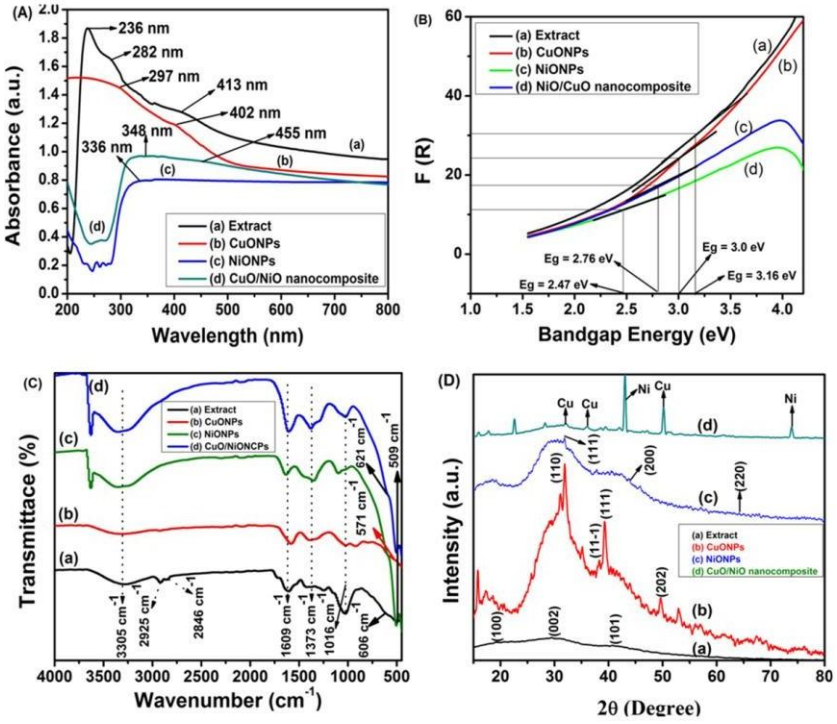

Figure 1. (A-D). (A) UV–Visible absorption spectra, (B) Tauc plot, (C) FT-IR spectra and (D) X-ray spectra of (a) Extract, (b) CuONPs, (c) NiONPs and (d) NiO/CuO nanocomposite

3.4 Surface Morphology characterization

Figure 2 (A-D) shows the surface morphology of the CuONPs study was investigated by SEM at 20 µM, 10 µM, 2 µM and 1 µM with different magnification. White agglomerate particles were obtained at low magnification at 20 µM as shown in Fig.2 (A). Very compact spherical particles were observed at higher magnification at 10 and 2 µM as shown in Fig.2 (B&C). The spherical shape of CuONPs was clearly recorded at highest magnification at 1 µM as shown in Fig.2 (D). Also, the percentage elements were analyzed by EDAX. Cu, O and C elements were presented in CuO NPs, which is evidenced for the preparation of CuO NPs as shown in Fig.2 (E).

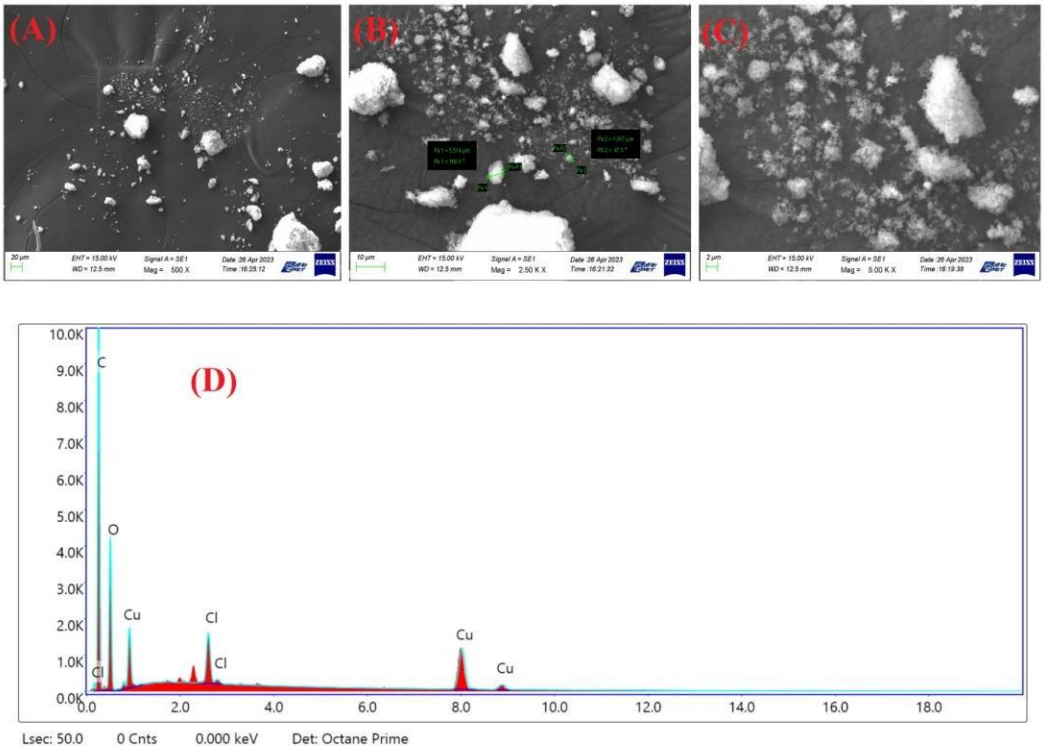

Figure 2. SEM images of NiONPs (A) 20 µM, (B) 10 µM, (C) 2 µM and (D) Energy dispersive spectra (EDS).

Figure 3(A-C) shows SEM images of NiONPs characterized at 10 µM, 2 µM and 2 µM with various magnifications. The white spherical shape of particles was obtained at low magnification 10 µM as shown in Fig.3 (A). The spherical shape was obtained at high magnification 2 µM as shown in Fig.3 (B). White particles of spherical shape 2 µM highest magnification as shown in Fig.3(C). Ni, O and C elements in NiONPs due to the formation of nickel oxide nanoparticles are shown in Fig.3 (D).

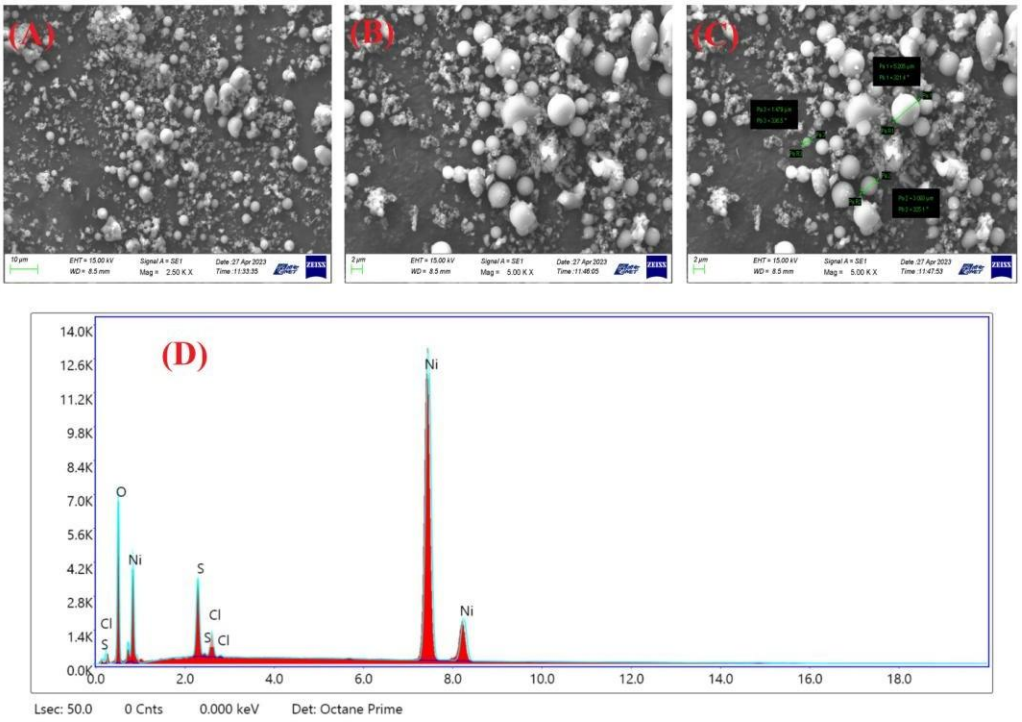

Figure 3. SEM images of CuONPs (A) 10 µM, (B) 2 µM, (C) 2 µM, and (D) Energy dispersive spectra (EDS).

SEM image of CuO/NiO nanocomposite revealed aggregated particles at 5 µM as shown in Fig.4 (A). It displayed un-uniform shape of particles when SEM was carried out at high magnification 2 µM as shown in Fig.4 (B). Therefore, at highest magnification 1 µM spherical shape of CuONPs attached to the NiONPs particles surface was shown in Fig.4(C). Figure 4(D) illustrates the EDAX spectrum of Cu, Ni, O and C elements in the CuO/NiO nanocomposite , confirming the formation of the CuO/NiO nanocomposite.

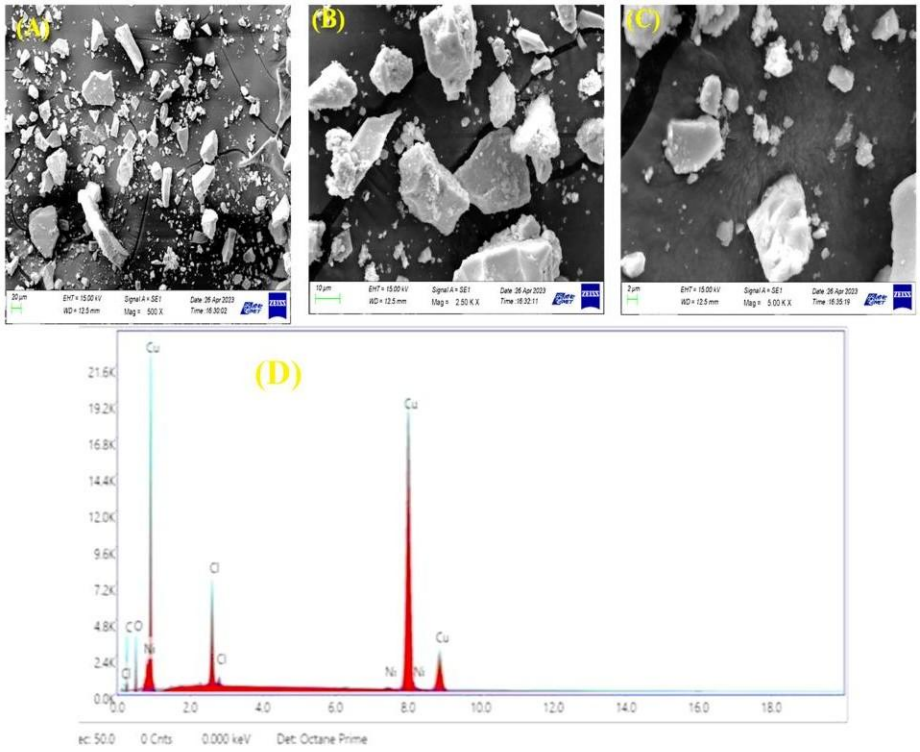

Figure 4. SEM images of NiO/CuO nanocomposite (A) 5 µM, (B) 2 µM, (C) 1 µM and (D) Energy dispersive spectra (EDS).

3.5 Transmission Electron Microscope

A transmission Electron microscope was used to evaluate the material's size and shape. The TEM images of CuO/NiO nanocomposite were uniform distributed spherical particles observed at 100 nm and 50 nm as shown in Fig.(A&B). The large spherical shape of copper particles were coated on NiO recorded at high magnification (10 nm) as shown in Fig.(C&D). At the highest magnification of 10 nm, the spherical shape of copper particles was clearly coated on NiO displayed as shown in Fig.(E). The SAED pattern has also confirmed the crystallinity of CuO/NiO nanocomposite as shown in Fig.(F).

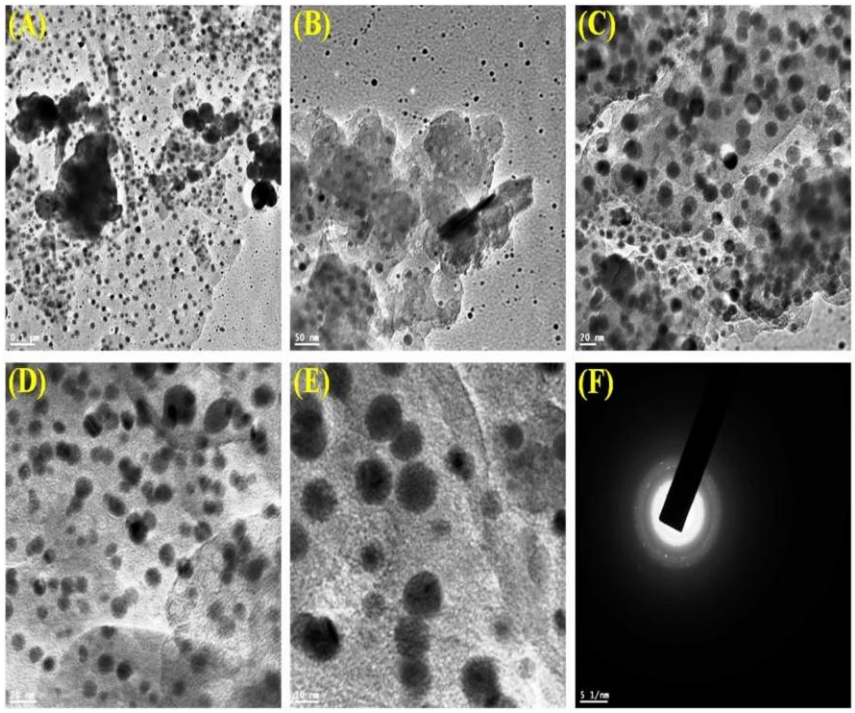

Figure 5. (A-D). TEM images of the CuO/ZnO nanocomposite (A) 50 nm, (B) 20 nm, (C) 10 and (D) 5 nm . (E) SAED pattern of CuO/ZnO nancomposite.

3.6 Photocatalytic Application

Figure 5(A-C) shows the photocatalytic degradation of cationic MB dye with (A) NiONPs, (B) CuONPs and (C) CuO/NiO nanocomposite under visible light irradiation at time range 0 to 90 min. The concentration of dye was effectively monitored by UV-visible spectroscopy. Initially, the photocatalysts of NiONPs, CuONPs and CuO/NiO nanocomposite reached adsorption with MB under dark condition at 0 min. The NiONPs photocatalyst for the degradation of MB was investigated with visible light irradiation from 0 to 90 min and the degradation intensity of MB was observed to peak at 674 nm. It did not fully reduce the peak intensity as shown in Figure 5 (A). Figure 5(B) shows that CuONPs were degraded following MB under visible light irradiation from 0 to 90 min, and it showed a better photocatalytic activity than NiONPs.Figure 5(C) shows the complete decolorization of the degradation of MB with CuO/NiO nanocomposite as a photocatalyst under visible light irradiation from 0 to 90 min [60, 61]. The photocatalytic degradation efficiency was calculated by using η (%) = C_0-C_t/C_0 x 100, where C_0 is the initial concentration at 0 min and C_t is the final concentration at 90 min. 96 % of MB degradation was conducted with CuO/NiO nanocomposite than CuONPs (92 %) and

NiONPs (85 %) as shown in Fig.6(A). CuO/NiO nanocomposite showed lower band gap energy and better degradation efficiency due to better doping of CuONPs in NiONPs. The kinetic rate constant for MB degradation was estimated for various photocatalysts NiONPs, CuONPs and CuO/NiO nanocomposite using the first –order rate equation [62].

$$\ln(C_t/C_0) = -kt \quad \text{.....(2)}$$

Where C_0 is the initial concentration of MB before visible light irradiation and Ct is the final concentrations after visible light irradiation time t. k is the kinetic rate constant (min^{-1}). ln (C_t/C_0) vs t was used to calculate k by using the slope value. The kinetic rate constant of NiONPs (k = 0.4551 min^{-1}), CuONPs (k =0.4881 min^{-1}) and CuO/NiO nanocomposite (k = 0.5213 min^{-1}) were obtained from the Fig. 6B(a-c). In this CuO/NiO nanocomposite was proved to be good photocatalyst than CuONPs and NiONPs.

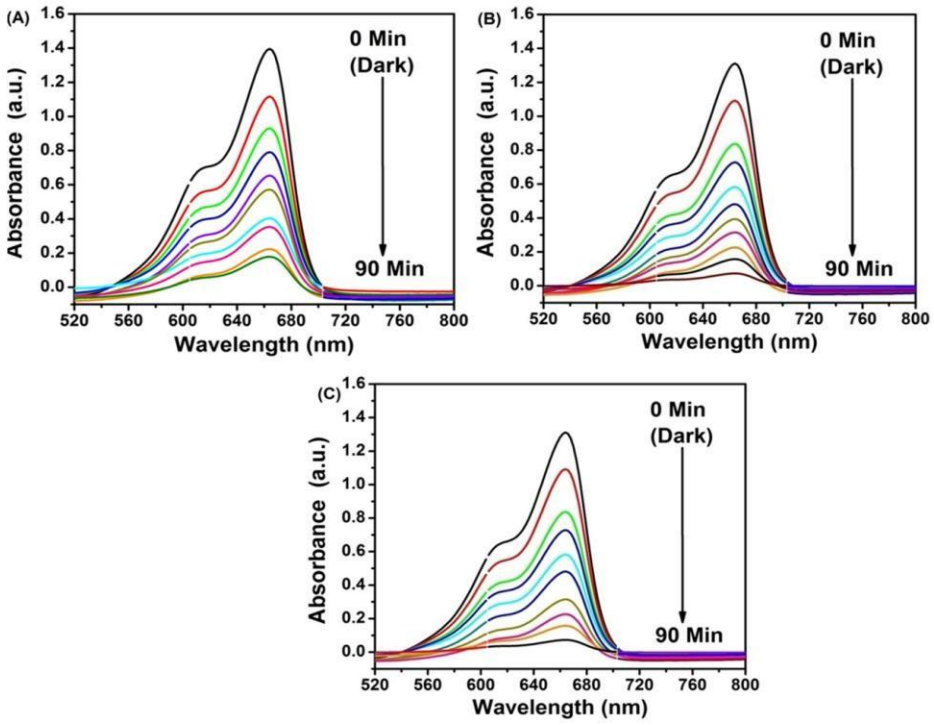

Figure 6. UV-vis spectra of (A) NiONPs, (B) CuONPs and (C) NiO/CuO nanocomposite the photocatalytic degradation of MB under visible light irradiation at various time intervals 0 to 90 min.

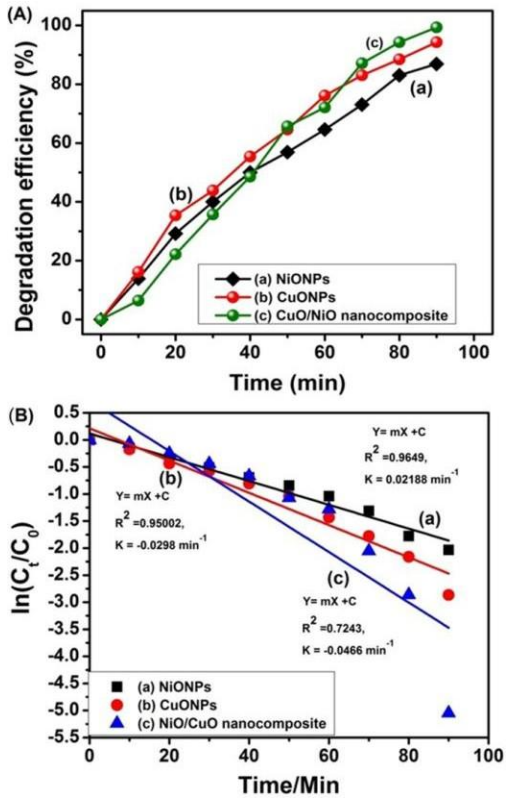

Figure 7. (A) Calibration plot of the degradation efficiency vs time and (B) plot of $\ln(C_t/C_0)$ vs time.

3.6. Photocatalytic degradation mechanism

Figure 7 shows the photocatalytic degradation mechanism of MB with CuO/NiO nanocomposite was conducted under visible light irradiation. The CuO/NiO nanocomposite works as a heterojunction photocatalyst with reduced electrons-holes recombination rate, with band gaps energy of CuO (1.42 eV) and NiO (2.4 eV) [63, 64]. CuO/NiO nanocomposite produces the electrons-holes at conduction band (CB) and Valence band (VB). The band gap energy of NiO was higher than CuO so that photoexcited electrons (e^-) moved from the CB band NiO from CB of CuO after visible light absorption, While holes (h^+) was transferred from VB of NiO to VB of CuO [65]. Then oxygen molecules in the MB solution combine with e^- to form superoxides radicals ($^{\bullet}O_2$-) and h^+ reacted with H_2O to generate the hydroxyl radicals ($^{\bullet}OH$). $^{\bullet}O_2^-$ and $^{\bullet}OH$ are powerful oxidizing radicals to greatly degrade the MB to complete mineralization [66]. h^+ worked as reductant to decompose MB to degrade by-products and mineralization. Further, photocatalytic degradation mechanism of MB by CuO/NiO nanocomposite under visible light irradiation is given below.

$$NiO/CuO + hv \longrightarrow NiO/CuO\ [h^+\ (VB) + e^-\ (CB)]$$

$$NiO/CuO\ [h^+\ (VB) + e^-\ (CB)] \longrightarrow NiO\ h^+\ (VB) + CuO\ (e^-)\ (CB)]$$

$$NiO\ (e^-) + O_2 \longrightarrow {}^{\bullet}O_2^-$$

$$CuO\ (h^+) + H_2O \longrightarrow OH^{\bullet} + H^+$$

$$\cdot O_2^- + MB \longrightarrow \text{degraded byproducts + mineralization}$$

$$\cdot OH + MB \longrightarrow \text{degraded byproducts + Mineralization}$$

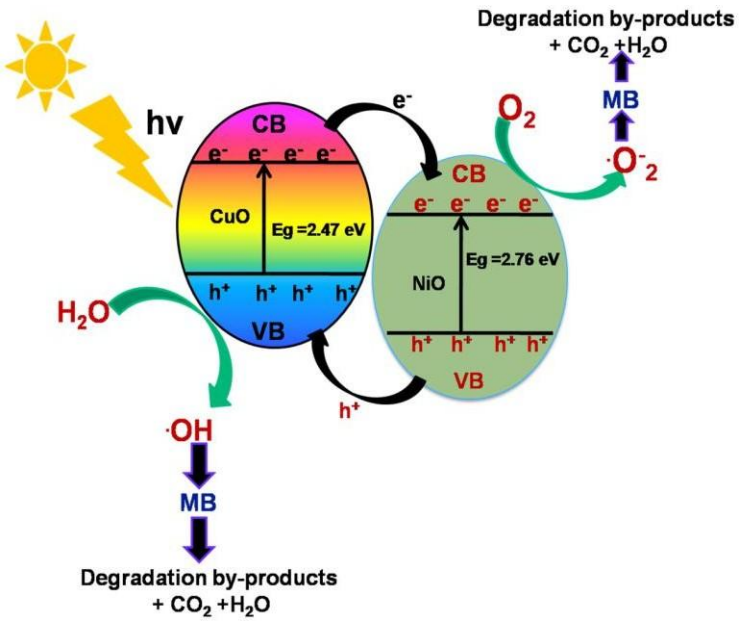

Figure 8. Photocatalytic Degradation Mechanism of MB by NiO/CuO Nanocomposite under Visible Light Irradiation.

3.7 Anti-bacterial activity of the samples

CuONPs, NiONPs and CuO/ZnO nanocomposite samples were tested for the anti-bacterial activity against *Escherichia coli (E.coli*) and *Staphylococcus.aureus (S.aureus)* bacteria by Disc diffusion method. The antibacterial activities in presence of 120 µg/mL of the samples were shown in Figure (A-D). As noted, The CuONPs and NiONPs samples were displayed the weak anti-bacterial activity against both *Escherichia coli* (*E.coli*) and *Staphylococcus aureus (S.aureus)* bacteria with No Zone formation for CuONPs and NiONPs for *S.aureus* and 13 mm of CuONPs and 14 mm of NiONPs for *E.coli).* CuONPs and NiONPs prepared by using

Sapthodena camptanulata leaf extracted to reduced antibacterial activity. Moreover, CuO/NiO nanocomposite was exhibited the higher anti-bacterial activities with a Zone formation of 20 mm for *E.coli* and 18 mm for *S.aureus* bacteria as shown in Fig.(C&D)

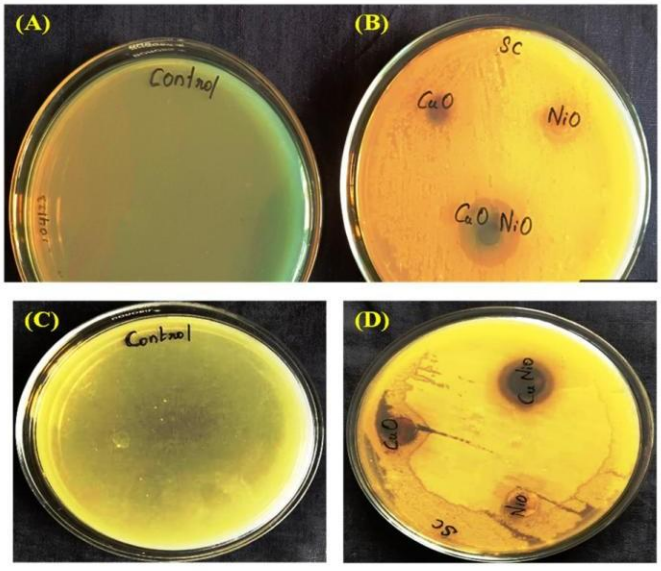

(E)

Pathogenic bacteria	Control	CuONPs	NiONPs	NiO/CuO nanocomposite
E.Coli	-	13 mm	14 mm	20 mm
S.aureus	-	-	-	18 mm

Figure 9. (A-E). Anti-bacterial activities of the CuONPs, NiONPs, CuO/NiO nanocomposite samples against *E. coli (A&B)* and *S. aureus* (C&D) and (E) Comparison Result.

4. Conclusion

NiO/CuO nanocomposite were successfully prepared through facile hydrothermal method with *Sapthodena camptanulata* leaf extract. The synthesis of NiO NPs, CuO NPs, and CuO-NiO NCs are indicated by UV-vis absorption peaks at 336, 297, and 347 nm, respectively. The biofabrication of the NPs by the action of several phytochemicals with various functional groups present in the leaf extract was confirmed by FT-IR experiments. The crystalline nature, phase composition, and purity of the synthesised nanoparticles were all confirmed by the XRD patterns. SEM image clearly indicated that the NiO particles coated on CuO. TEM result showed NiO/CuO nanocomposite was slightly agglomerated in spherical shape with size around 20–50 nm. The NiO/CuO nanocomposite can be efficiently used as a heterogeneous photocatalyst for the decomposition of the MB dye. The degradation percentage of MB was higher for NiO/CuO than CuONPs and NiONPs. The superior photocatalytic performance was exhibited by the

NiO/CuO nanocomposite owing to the synergistic effect between CuO and NiO. NiO/CuO nanocomposite was shown the good anti-bacterial activities against both *(E.coli)* and (*S.aureus)* bacteria than ZnONPs and CuONPs.

Acknowledgement

We thank DST-FIST, India for the IR and UV instrumental facilities at the PG and Research centre, Department of Chemistry, Sri Paramakalyani College, Alwarkurichi. We thank Dr. G. Ramanathan, Deparment of Microbiology, Sri Paramakalyani College for antibacterial studies.

Conflicts of interest

The authors declare no conflict interest.

Reference

[1] Bora LV, Mewada RK. Visible/solar light active photocatalysts for organic effluent treatment: fundamentals, mechanisms and parametric review. Renew Sustain Energy Rev **2017**, 76, 1393e421.

[2] Chena L, Zhanga Z, Wanga Y, Guana Y, Denga K, Lva K, et al. Photocatalytic properties and electrochemical characteristic of a novel biomimetic oxygenase enzyme photocatalyst iron (II) tetrahydroxymethyl tetra(1,4-dithiin) porphyrazine for the degradation of organic pollutants. J Mol Catal Chem **2013**, 372, 114e20.

[3] Wang Z, Gao M, Li X, Ning J, Zhou Z, Li G. Efficient adsorption of methylene blue from aqueous solution by graphene oxide modified persimmon tannins. Mater Sci Eng C **2020**, 108, 110196.

[4] Andrade Siqueira TC, Zanette da Silva I, Rubio AJ, Bergamasco R, Gasparotto F, Aparecida de Souza Paccola E, et al. Sugarcane bagasse as an efficient biosorbent for methylene blue removal: kinetics, isotherms and thermodynamics. Int J Environ Res Publ Health **2020**, 17, 526.

[5] Kheraa RA, Iqbal M, Ahmad A, Hassan SM, Nazir A, Kausar A, et al. Kinetics and equilibrium studies of copper, zinc, and nickel ions adsorptive removal on to Archontophoenix alexandrae: conditions optimization by RSM. Desalination Water Treat **2020**, 201, 289e300.

[6] Liu QX, Zhou YR, Wang M, Zhang Q, Ji T, Chen TY, et al. Adsorption of methylene blue from aqueous solution onto viscose-based activated carbon fiber felts: kinetics and equilibrium studies. Adsorpt Sci Technol **2019**, 37, 312e32.

[7] Lau YY, Wong YS, Teng TT, Morad N, Rafatullah M, Ong SA. Degradation of cationic and anionic dyes in coagulationflocculation process using bi-functionalized silica hybrid with aluminum-ferric as auxiliary agent. RSC Adv **2015**, 5, 34206e15.

[8] Tir M, Moulai-Mostefa N, Nedjhioui M. Optimizing decolorization of methylene blue dye by electrocoagulation using Taguchi approach. Desalination Water Treat **2015**, 55, 2705e10.

[9] El-Ashtoukhy ESZ, Fouad YO. Liquid-liquid extraction of methylene blue dye from aqueous solutions using sodium dodecyl- benzenesulfonate as an extractant. Alex Eng J **2015**, 54, 77e81.

[10] Kim S, Yu M, Yoon Y. Fouling and retention mechanisms of selected cationic and anionic dyes in a Ti3C2Tx MXeneultrafiltration hybrid system. ACS Appl Mater Interfaces **2020**, 12, 16557e65.

[11] Maas ASVD, Da Silva NJR, Da Costa ASV, Barros AR, Bomfeti CA. The degradation of methylene blue dye by the strains of pleurotus sp. with potential applications in bioremediation processes. Rev Ambient Agua **2018**, 13, e2247e56.

[12] Fahmy A, El-Zomrawy A, Saeed AM, Sayed AZ, Ezz El- Arab MA, Shehata HA. Modeling and optimizing acid orange 142 degradation in aqueous solution by nonthermal plasma. Chemosphere **2018**, 210, 102e9.

[13] Imron MF, Kurniawan SB, Soegianto A, Wahyudianto FE. Phytoremediation of methylene blue using duckweed (Lemna minor). Heliyon **2019**, 5, e02206-e02211.

[14] Athanasekou CP, Moustakas NG, Morales-Torres S, Pastrana- Martı´nez LM, Figueiredo JL, Faria JL, et al. Ceramic photocatalytic membranes for water filtration under UV and visible light. Appl Catal, B: Environ **2015**, 178, 12e9.

[15] Crini G, Lichtfouse E. Advantages and disadvantages of techniques used for wastewater treatment. Environ Chem Lett **2019**, 17, 145e55.

[16] Yang L, Duan W, Jiang H, Luo S, Luo Y. Mesoporous TiO2@Ag3PO4 photocatalyst with high adsorbility and enhanced photocatalytic activity under visible light. Mater Res Bull **2015**, 70, 129e36.

[17] Ali S, Khan SA, Khan I, Yamani ZH, Sohail M, Morsy MA. Surfactant-free synthesis of ellipsoidal and spherical shaped TiO2 nanoparticles and their comparative photocatalytic studies. J Environ Chem Eng **2017**, 5, 3956e62.

[18] Barnes RJ, Molina R, Xu J, Dobson PJ, Thompson IP.Comparison of TiO2 and ZnO nanoparticles for photocatalytic degradation of methylene blue and the correlated inactivation of gram-positive and gram-negative bacteria. J Nanopart Res **2013**, 15, 1432.

[19] Khan I, Qurashi A. Sonochemical-assisted in situ electrochemical synthesis of Ag/a-Fe2O3/TiO2 nanoarrays to harness energy from photoelectrochemical water splitting. ACS Sustain Chem Eng **2018**, 6, 11235e45.

[20] Ramesh M, Chander Rao MP, Anandan S, Nagaraja H. Adsorption and photocatalytic properties of NiO nanoparticles synthesized via a thermal decomposition process. J Mater Res **2008**, 33, 601e10.

[21] Singh, J., Manna, A. K. & Soni, R. K. Sunlight driven photocatalysis and non-enzymatic glucose sensing performance of cubic structured CuO thin films. *Appl. Surf. Sci.* **2020**, 530, 147258.

[22] Fardood ST, Moradnia F, Moradi S, Forootan R, Zare FY, Heidari M. Eco-friendly synthesis and characterization of a- Fe2O3 nanoparticles and study of their photocatalytic activity for degradation of Congo red dye. Nanochem Res **2019**, 4(2), 140e7.

[23] Ni L, Du C, Wu H, Li Y, Li X, Xu C. Preparation and characterization of Fe2O3/Bi2WO6 composite and photocatalytic degradation mechanism of microcystin-LR. Water Sci Eng **2021**, 14, 109e18.

[24] Martínez-Vargas, B.L.; Cruz-Ramírez, M.; Díaz-Real, J.A.; Rodríguez-López, J.; Bacame-Valenzuela, F.J.; Ortega-Borges, R.; Reyes-Vidal, Y.; Ortiz-Frade, L. Synthesis and characterization of n-ZnO/p-MnO nanocomposites for the photocatalytic degradation of anthracene. J. Photochem. Photobiol. A **2019**, 369, 85–96

[25] Yin X, Liu L, Ai F, Enhanced Photocatalytic Degradation of Methylene Blue by WO_3 Nanoparticles Under NIR Light Irradiation, Front. Chem., 01 July 2021, Sec. Nanoscience , **2021,** 9

[26] Arumugam M, Choi MY. Effect of operational parameters on the degradation of methylene blue using visible light active BiVO4 photocatalyst. Bull Korean Chem Soc **2020**, 41, 304e9.

[27] Bhattacharjee, Archita, Ahmaruzzaman M, .Green Synthesis of SnO_2 Nanoparticles and Its Application as Photocatalyst in the Degradation of Dye , Source: Advanced Science Letters, **2016**, 22, 216-218(3)

[28] S. Rajendran,M. Mansoob Khan, F. Gracia, J. Qin, V.K. Gupta, S. Arumainathan, Ce3+- ion-induced visible-light photocatalytic degradation and electrochemical activity of ZnO/CeO2 nanocomposite, Sci. Rep. **2016**, 6, 31641.

[29] Zhang D, Zhang, Zhang G, Liu T. Construction of magnetic core-ring-structured porous hexagonal NiCo2O4 nanoplates/carbon fibers hybrid with enhanced visiblelight photocatalytic performance. J Mater Sci **2019**, 54, 7617e27.

[30] Sabouri, Z.; Akbari, A.; Hosseini, H.A.; Darroudi, M. Facile green synthesis of NiO nanoparticles and investigation of dye degradation and cytotoxicity effects. J. Mol. Struct. **2018**, 1173, 931–936.

[31] Yu C, Wen M, Tong, Z, Li S, Yin Y, Liu X, Li Y, Liang T, Wu Z. Dionysiou, D.D. Synthesis and enhanced photo-catalyticperformance of 0D/2D CuO/tourmaline composite photocatalysts. Beilstein J. Nanotechnol. **2020**, 11, 407–416

[32] Mohammed A. Mannaa, ,Khaled F. Qasim, Fares T. Alshorifi, Salah M. El-Bahy, Reda S. Salama, Role of NiO Nanoparticles in Enhancing Structure Properties of TiO_2 and Its Applications in Photodegradation and Hydrogen Evolution, *ACS Omega* **2021**, 6, 45, 30386–30400.

[33] Changlin YU, Kai YA, Qing SH, Jimmy CY, Fangfang CA, Xin LI. Preparation of WO_3/ZnO Composite Photocatalyst and Its Photocatalytic Performance, Chinese Journal of Catalysis, **2011**, 32, 555-565.

[34] Fouda A, Salema S S, Wassel A R, Hamza M F, Shaheen T I,Optimization of green biosynthesized visible light active CuO/ZnO ano-photocatalysts for the degradation of organic methylene blue dye, Heliyon **2020**, 6, e04896.

[35] Liu J, Lin C, Yao H, Zhang S, Fang D, Jiang L, Wang D, Zhang Z, Wang J, Construction of high-proportion ternary dual Z-scheme Co3O4/NiCo2O4/NiO photocatalytic system via incomplete solid phase chemical reactions of Co(OH)2 and Ni(OH)2 for organic pollutant degradation with simultaneous hydrogen production, Journal of Power Sources, **2021**, 506, 230159.

[36] Kumari, V., Mphahlele-Makgwane, M.M., Makgwane, P.R. Ultrasonically Pd functionalized, surface plasmon enhanced ZnO/CeO_2 heterostructure for degradation of organic pollutants in water. *Eur. Phys. J. Plus* **2022**, 137, 565.

[37] Rahman Z U, Shah U, Alam A, ShahZ , Shaheen K , Khan S B, Khan S A, Photocatalytic degradation of cefixime using CuO-NiO nanocomposite Photocatalyst, Inorganic Chemistry Communications **2023**, 148, 110312.

[38] Xu H, Zhu G, Zheng D, Xi Ch, Xu X, Shen X, Porous CuO superstructure: precursormediated fabrication, gas sensing and photocatalytic properties, J. Colloid Interface Sci. **2012**, 383, 75–81.

[39] Gondal M.A., Sayeed M.N., Seddigi Z., Laser enhanced photo-catalytic removal of phenol from water using p-type NiO semiconductor catalyst, J. Hazard. Mater. **2008**, 155, 83–89.

[40] Muhambihai P, Rama V, Subramaniam P. Photocatalytic degradation of aniline blue, brilliant green and direct red 80 using NiO/CuO, CuO/ZnO and ZnO/NiO nanocomposites. Environmental Nanotechnology, Monitoring & Management. Environmental Nanotechnology, Monitoring & Management, **2020**, 14, 100360.

[41] Nazar, S.; Hussain, M.A.; Khan, A.; Muhammad, G.; Tahir, M.N. Capparis decidua Edgew (Forssk.): A comprehensive review of its traditional uses, phytochemistry, pharmacology and nutrapharmaceutical potential. Arab. J. Chem. **2020**, 13, 1901–1916*]*.

[42] Premalatha, N.; Miranda, L.R. Surfactant modified ZnO–Bi2O3 nanocomposite for degradation of lambda- cyhalothrin pesticide in visible light: A study of reaction kinetics and intermediates. J. Environ. Manag. **2019**, 246, 259–266.

[43] Jonidi-Jafari, A.; Shirzad-Siboni, M.; Yang, J.K.; Naimi-Joubani, M.; Farrokhi, M. Photocatalytic degradation of diazinon with illuminated ZnO-TiO2 composite. J. Taiwan Inst. Chem. Eng. **2015**, 50, 100–107.

[44] Dina F. Katowah Sayed M. Saleh Sara A. Alqarni4, Reham Ali, Gharam I. Mohammed1 & Mahmoud A. Hussein, Network structure-based decorated CPA@CuO hybrid nanocomposite for methyl orange environmental remediation, Scientific Reports **2021**, 11, 5056

[45] Bhuvaneswari P, Shanmugavadivu T, Sabeena G, Annadurai G, Sindhuja E. Synthesis and characterization of chitoson with silica (CS) nanocomposite with enhanced antibacterial activity, Int. J. Res. Pharm. Sci., **2022**, 13(1), 1-8.

[46] Shanmugavadiv T, Bhuvaneswari P, Sabeena G, Annadurai G, Sindhuja E. Synthesis and characterization of chitoson with monomorllonite nanocomposite (CNC) with enhanced antibacterial activity. J. Bio. & Env. Sci. **2022**, 21, 148-156.

[47] Renuga D, Jeyasundari J, Athithan AS S, Jacob Y B A, Synthesis and characterization of copper oxide nanoparticles using Brassica oleracea var. italic extract for its antifungal application. Mater. Res. Express **2020**, 7, 045007.

[48] Naika H.R. Lingaraju K. Manjunath K. Kumar D. Nagaraju G. Suresh D. and Nagabhushana H. J. Taibah Univ. Sci., **2015**, 9, 7

[49] Thamer N.A, Mufin N.Q, Al-Rubae S.H.N, Optimization Properties and Characterization of Green Synthesis of Copper Oxide Nanoparticles Using Aqueous Extract of Cordia myxa L. Leaves, Asian Journal of Chemistry; **2018**, 30, 1559-1563,

[50] Diallo A, Kaviyarasua K. Ndiayea S, Mothudia B. M, Ishaqa A, Rajendran V. and Maaza M, Structural, optical and photocatalytic applications of biosynthesized NiO, Nanocrystals, - Green Chemistry Letters And Reviews, **2018,** 11, 2, 166–175.

[51] Zhao, J.; Liu, H.; Zhang, Q. Preparation of NiO Nanoflakes Under Different Calcination Temperatures and their Supercapacitive and Optical Properties. Appl. Surf. Sci. **2017,** 392, 1097–1106.

[52] Rahdar A, Aliahmad M, Azizi Y, Keikha N, Moudi M and Keshavarzi F. CuO-NiO Nano composites: Synthesis, Characterization, and Cytotoxicity evaluation. Nanomedicine Res. J. 2, 78.

[53] Firisa S. G, Muleta G. G, and Yimer A. A, Synthesis of Nickel Oxide Nanoparticles and Copper-Doped Nickel Oxide Nanocomposites Using Phytolacca dodecandra L'Herit Leaf Extract and Evaluation of Its Antioxidant and Photocatalytic Activities, is: ACS Omega **2022**, 7, 44720−44732.

[54] Gopalakrishnan K Antibacterial activity of Cu_2O nanoparticles on E. coli sythesised from tridax procumbens leaf extract and surface coating with polyaniline Digest J.Nanomaterials and Biostructures. **2012**, 7 833–9.

[55] Nayak R, Ali F.A, Mishra D.K, Ray D, Aswal V, Sahoo S.K, Nanda B. Fabrication of CuO nanoparticle: An efficient catalyst utilized for sensing and degradation of phenol. J. Mater. Res. Technol. **2020**, 9, 11045–11059.

[56] Saravanakkumar, D. Synthesis of NiO doped ZnO/MWCNT nanocomposite and its characterization for photocatalytic & antimicrobial applications. J. Appl. Phys. **2018**, 10, 73–83.

[57] Katowah D F, Saleh S M, Alqarni S A, Ali R, Mohammed G I & Hussein M I, Network structure‐ based decorated CPA@CuO hybrid nanocomposite for methyl orange environmental remediation, Scientific Reports **2021**, 11, 5056.

[58] Sagadevan S, Podder J. Investigations on structural, optical, morphological and electrical properties of nickel oxide nanoparticles. Int J Nanoparticles (IJNP) **2015**, 8, 289e301.

[59] Kumar A, Kumar A, and Krishnan V. Perovskite Oxide Based Materials for Energy and Environment-Oriented Photocatalysis. ACS Catal. **2020**, 10, 10253–10315.

[60] Kaneco S, Li N, Itoh K.-K, Katsumata H, Suzuki T, Ohta K, Titanium dioxide mediated solar photocatalytic degradation of thiram in aqueous solution: Kinetics and mineralization. Chem. Eng. J. **2009**, 148, 50–56.

[61] Molla M.A.I, Ahsan S, Tateishi I, Furukawa M, Katsumata H, Suzuki T, Kaneco S. Degradation, Kinetics, and Mineralization in the solar photocatalytic treatment of aqueous amitrole solution with titanium dioxide. Environ. Eng. Sci. **2018**, 35, 401–407.

[62] Prabakaran E and Pillay K. Self-Assembled Silver Nanoparticles Decorated on Exfoliated Graphitic Carbon Nitride/Carbon Sphere Nanocomposites as a Novel Catalyst for Catalytic Reduction of Cr(VI) to Cr(III) from Wastewater, and Reuse for Photocatalytic Applications, ACS Omega **2021**, 6, 51, 35221–35243.

[63] Chabri S, Dhara A, Show B, Adak D, Sinha A, Mukherjee N. Mesoporous CuO-ZnO p-n heterojunction based nanocomposites with high specific surface area for enhanced photocatalysis and electrochemical sensing. Catal. Sci. Technol. **2016**, 6, 3238–3252.

[64] Hansen B.J, Kouklin N, Lu G.H, Lin I, Chen J.H, Zhang X, Transport, analyte detection, and opto-electronic response of p-Type CuO nanowires. J. Phys. Chem. C **2010**, 114, 2440–2447.

[65] Zhang J.N, Chen T.H, Yu J.H, Liu C, Yang Z.B, Lu H.B, Yin F, Gao J.Z, Liu Q.R, Zhang X.W, Enhanced photocatalytic activity of flowerlike CuO-ZnO nanocomposites synthesized by one-step hydrothermal method. J. Mater. Sci. **2016**, 27, 10667–10672.

[66] Harish S, Archana J, Sabarinathan M, Navaneethan M, Nisha K.D, Ponnusamy S, Muthamizhchelvan C, Ikeda H, Aswal D.K, Hayakawa Y, Controlled structural and compositional characteristic of visible light active ZnO/CuO photocatalyst for the degradation of organic pollutant. Appl. Surf. Sci. **2017**, 418, 103–112.